Altered excitation-inhibition balance in the somatomotor and default mode network in multiple sclerosis

Gaia Zin, Guy Nagels, Jeroen Van Schependom, Thanos Manos

Altered excitation-inhibition balance in the somatomotor and default mode network in multiple sclerosis

Gaia Zin [1,2,3,*], **Guy Nagels** [1,2,4], **Jeroen Van Schependom** [1,2] **and Thanos Manos** [3,*]

[1] *AIMS, Center for Neurosciences, Vrije Universiteit Brussel, Brussel, Belgium.*
[2] *Department of Electronics and Informatics (ETRO), Vrije Universiteit Brussel, Brussel, Belgium.*
[3] *ETIS Lab, ENSEA, CNRS, UMR8051, CY Cergy-Paris University, Cergy, France.*
[4] *NEUR, Center for Neurosciences, UZ Brussel, Vrije Universiteit Brussel, Brussels, Belgium.*

Correspondence*:
Gaia Zin
gaia.zin@vub.be

Thanos Manos, ETIS Lab, ENSEA, CNRS, UMR8051, CY Cergy-Paris University, Cergy, France, thanos.manos@cyu.fr

ABSTRACT

Introduction: The balance between excitatory and inhibitory (E/I) neural processes is a fundamental principle of brain function, and its disruption has been implicated in the pathophysiology of multiple sclerosis (MS). In vivo assessment of E/I balance has traditionally relied on electrophysiological measures, and despite the abundance of fMRI data on MS, no fMRI-based technique has so far been presented to measure E/I balance in MS.

Methods: Recently, a novel MRI-based method has been introduced to estimate E/I balance by integrating functional MRI and diffusion weighted imaging data. We use this approach to study E/I balance in MS at a global (over the whole head) and at the local level of specific resting state networks affected by MS: the somatomotor and Default Mode network (DMN). Furthermore, we perform the analysis using three different atlases: the Schaefer atlas, which is functionally defined, and the Automatic Anatomical Labeling (AAL) and Desikan Killany (DK) atlas, which are defined based on structural features.

Results: Our findings reveal a significant alteration in E/I balance within the somatomotor and default mode networks when using the functionally defined Schaefer atlas, suggesting a network-specific dysfunction in MS. We also find that the E/I balance inferred within the somatomotor network correlates with motor fatigue.

Conclusions: This study demonstrates a promising framework for investigating E/I balance alterations in neurological disorders and paves the way for validation in larger cohorts.

Keywords: Multiple sclerosis, multimodal MRI, functional connectivity, structural connectivity, resting-state informed structural connectome, excitation-inhibition balance

1 INTRODUCTION

Multiple sclerosis (MS) is a chronic neuroinflammatory disease that primarily affects the central nervous system and is the leading cause of non-traumatic neurological disability in young adults [1] and, in particular, women (see e.g., [2]). The pathophysiology of MS is driven by immune-mediated processes that lead to inflammation, demyelination, and neuronal loss (neurodegeneration) [3, 4]. These processes result in a wide range of symptoms, including fatigue and cognitive impairment, see e.g., [5].

A fine balance between excitation and inhibition in the brain, also referred to as Excitation/Inhibition (E/I) balance, is crucial for proper information processing and healthy neuronal function, see e.g., [6, 7]. Disruptions in E/I balance have been observed in various neurological disorders, including schizophrenia [8, 9], Alzheimer's disease [10, 11], and autism spectrum disorder [12, 13].

In MS, neuronal and synaptic loss could result in a shift in E/I balance [14, 15]. Post-mortem analyses of motor cortex tissue suggest a preferential loss of inhibitory interneurons in the grey matter [16]. Consistent with this, experimental autoimmune encephalomyelitis studies demonstrate a pro-excitatory shift in the motor cortex [17]. Furthermore, Huiskamp et al. [14] observed a loss of both excitatory and inhibitory synapses in post-mortem tissue. These synaptic alterations were subsequently incorporated into a computational model to study large-scale network dynamics in people with multiple sclerosis (pwMS). The authors found that the inhibitory synaptic loss alone impacts the empirical neuronal activity and functional connectivity more profoundly. We also note that in-vivo studies of E/I alterations in MS predominantly rely on electrophysiological modalities like electroencephalography (EEG) and magnetoencephalography (MEG) (see e.g., [18]). However, despite the abundance of fMRI data of pwMS, no fMRI-based study has been used to infer E/I changes in MS.

Recently, there has been growing interest in the interplay between structural and functional connectivity (see e.g., [19]). Structural connectivity can constrain functional dynamics, while functional mechanisms can reshape anatomical pathways through plasticity and neuromodulation [20, 21]. To capture these interactions, Ajilore et al. [22] introduced the concept of a hybrid resting-state structural connectivity (rsSC) as a metric encapsulating the interplay between structural and functional connectivity. The rsSC integrates information from diffusion-weighted imaging (DWI) and resting-state fMRI data. Fortel et al. [23] proposed a similar multimodal rsSC based on a model from statistical mechanics. Through this modeling framework, the entries of the new rsSC are linked to macroscopic E/I dynamics. The authors have used it to study E/I alterations in Alzheimer's disorder. In particular, female carriers of the apolipoprotein E epsilon 4 exhibited more susceptibility to network disruption, given an increase in excitations, compared to male carriers [24]. Later studies incorporate E/I estimates at both region-of-interest (ROI) and whole-atlas levels into mixed-effects models accounting for sex [25] and disease progression over time [11]. These findings suggest that the rsSC metric reliably captures biologically meaningful differences in E/I balance. Recently, in Manos et al. [26], the authors used such hybrid (structural and functional) connectivity to study whole-brain dynamics and simulated efficiently BOLD signals and functional connectivity with a Kuramoto model. They found that simulations of dynamical models using rsSC to define brain node interactions, instead of classical SC matrices, showed significantly higher correspondence with empirical fMRI data.

This multimodal approach is particularly interesting for MS, where functional brain reorganization likely follows structural damage in the disorder [27]. In particular, we are interested in measuring E/I imbalance both at a global level (whole brain) and at a local level of specific Resting State Networks (RSNs) affected

by MS. We focus on two functional networks that play a role in MS: the somatomotor network and the DMN.

The DMN includes areas in the parietal, temporal, and frontal lobes [28]. Bonavita et al. [29] compared functional connectivity in DMN regions in three groups: healthy controls (HC), MS patients with no established cognitive impairment, and cognitively impaired MS patients. They found significantly weaker functional connectivity strength in people with MS (pwMS) compared to HCs, especially in the cingulate cortex. Other studies found DMN changes in functional connectivity strength when comparing different phenotypes of MS [30], and different levels of cognitive function and disease duration [31].

The somatomotor network also plays a key role in MS. In particular, it is associated with fatigue in MS [32], which is one of the most debilitating symptoms reported by patients. Furthermore, maladaptive reorganization of the somatomotor network associates with pain [33, 34]. Radetz et al. [35] observed a lower neurite density in the motor cortex of pwMS, which was correlated with higher excitability thresholds. Furthermore, in an experimental model of autoimmune encephalomyelitis, Potter et al. [17] found increased excitability in specific nodes of the somatomotor network, supporting a pro-excitatory shift in E/I balance within the somatosensory cortex.

In this study, we assessed whether the E/I balance - as captured through multimodal modelling of fMRI and DWI data - can capture differences between people with MS and healthy controls. In addition, we assessed the extent to which this variation depends on the parcellation atlas. Specifically, we employed a functional brain atlas—the Schaefer atlas—which parcellates the brain into regions based on patterns of functional activity, and hence allows for fast identification of well-defined functional networks. To further test our findings and initial intuition regarding the atlas choice, we also included two structural atlases: the AAL and DK atlas, both of which define regions according to anatomical features. By incorporating both functional and structural atlases, we can get insights into how atlas selection influences excitation/inhibition (E/I) estimates and group comparisons.

2 MATERIALS AND METHODS

2.1 Participants

This study includes data from 12 Healthy Controls (HC) and 24 people with MS (pwMS). All the subjects are female, and the data collection resided within the UZ Brussel. The groups are matched in sex, age, and years of education **Table** 1. The MS group includes only individuals with relapsing-remitting MS, whose diagnosis matches the revised McDonald criteria [36] and have an Expanded Disability Status Score (EDSS) less than 6. Each subject was evaluated with the Fatigue Scale for Motor and Cognitive Functions (FSMC), the Symbol Digit Modalities Test (SDMT), the Controlled Oral Word Association Test (COWAT), and the Brief Visuospatial Memory Test–Revised scores (BVMT-R).

2.2 Data acquisition

MRI data were acquired on a 3T Philips Achieva scanner at UZ Brussel. Resting-state fMRI used a 230 × 230 mm field of view, 48 slices, 1.8 × 1.8 × 2.7 mm voxels, flip angle 90°, TR = 3 s, and TE = 5 s. DWI was acquired on the same scanner with 32 non-collinear directions (b = 800 s/mm²) and one b0 volume, using a 250 × 250 mm field of view, 70 slices, 0.975 × 0.975 mm in-plane resolution, 2-mm slice thickness, TR = 5133 ms, and TE = 95 ms. Additional T1-weighted images were collected with a 240 × 240 mm field of view, 310 slices, 0.5-mm isotropic voxels, flip angle 8°, TR = 5.19 ms, and TE = 2.30 ms.

Table 1. Description of the clinical parameters of the HC and MS group. We show the mean and standard deviation of clinical parameters for both the HC and MS groups. For EDSS, we present the median and interquartile range (IQR). We applied the Shapiro-Wilk test to assess the normality of age, education, disease duration, EDSS, and cognitive scores in both groups. Most variables did not follow a normal distribution. Therefore, we used the non-parametric Mann-Whitney U test to compare the groups.

	HC	**pwMS**	**Group differences ($p-$values)**
N	12	24	-
Sex	F	F	-
Age (yrs)	41±13	48±11	0.15
Education (yrs)	14±4	13±3	0.54
Disease duration (yrs)	–	15±8	-
EDSS median [IQR]	–	2.5 [2-3.5]	-
Disability scores			
FSMC-motor	20±7	32±9	0.0008**
FSMC-cognitive	20±5	32±10	0.003**
SDMT	52±12	50±10	1.00
COWAT	80±20	81±26	0.75
BVMT-R	29±4	26±6	0.16

2.3 Ethics

Patient recruitment took place between 2015 and 2018. All participants provided written informed consent before inclusion. The ethical committees of the National MS Center Melsbroek and UZ Brussel approved the study (Commissie Medische Ethiek UZ Brussel, B.U.N. 143201423263, 2015/11). The study complied with all applicable ethical guidelines for research involving human participants.

2.4 DWI processing

We processed the Diffusion Weighted Images (DWI) using MRtrix3 and FSL [37, 38]. The preprocessing includes denoising, corrections for Gibbs ringing artifacts, eddy currents, and inhomogeneity distortions. The non-linear registration with the standard Montreal Neurological Institute (MNI) reference space was performed using ANTs [39]. The tracks are generated with a probabilistic diffusion tensor imaging algorithm, and seeded at the gray matter–white matter interface. After generating the tracks, the structural connectivity is calculated with the 'tck2connectome' function of MRtrix3, for each one of the investigated atlases.

2.5 fMRI processing

We perform the functional analysis using MATLAB 2024a and SPM12 [40]. Specifically, we apply the lesion segmentation tool from SPM12 to perform lesion growth and filling. We then use the resulting T1 lesion-filled image as a reference for projecting onto the MNI reference space and aligning it with the chosen brain atlas. For the fMRI data, we discard the first ten volumes to minimize startup effects. We apply motion and slice timing corrections to the remaining data. We discard any images that require more than 1 mm of translational or 0.0125 radians of rotational correction to maintain quasi-stationarity [41, 42]. We then linearly register the corrected fMRI images with the lesion-filled T1 image and compute the average signal for each region of interest (ROI). Next, we regress out the confounding effects of motion artifact, white matter and cerebrospinal fluid. After that, we apply bandpass filtering to the fMRI data within the frequency range of 0.009 Hz to 0.08 Hz. We calculate the Pearson correlation

coefficient between ROI pairs to assess functional connectivity. Finally, we discard any nonsignificant edges (threshold at $p = 0.05$).

2.6 Brain Atlases

In this section, we present the three brain atlases used in our study:

- The Schaefer atlas [43] defines regions of interest (ROIs) from a data-driven approach based on functional MRI recordings. It provides parcellations at multiple resolutions; we used the 100-ROI version. The ROIs follow the Yeo-7 network division [44] and thus map onto seven large-scale resting-state networks (RSNs): visual, somatomotor, dorsal attention, ventral attention (salience), limbic, frontoparietal, and default-mode.
- The Automatic Anatomical Labeling (AAL) atlas [45] comprises 90 cortical and 26 cerebellar ROIs. These ROIs are manually delineated based on sulcal anatomy and then labelled using automated procedures.
- The Desikan–Killiany atlas [46] contains 68 cortical ROIs manually defined using gyral anatomy. It was built from 40 MRI scans originally collected for Alzheimer's disease research, covering a wide age range (19–86 years) and capturing inter-individual variability relevant to neurodegeneration.

All atlases were obtained from Neuroparc [47], a standardized repository of human brain atlases. Neuroparc supplies atlases aligned to MNI space and organized at three spatial resolutions. While the ROIs of the (functional) Schaefer atlas are divided into RSNs by construction, this is not the case for the other two considered atlases. To align DK ROIs with the somatomotor network and DMN, we follow the partition into RSNs employed by Lee and Frangou [48]. For the AAL atlas, we overlap it with the Yeo-7 parcellation and compute, for each AAL ROI, the proportion of voxels that fall within each Yeo-defined network. We then select, for each RSN, the minimal voxel-percentage threshold that reliably represents that network; the optimal threshold varies across RSNs. We provide a detailed description of this workflow in Section 3 of the Supplementary Material.

2.7 Calculation of hybrid rsSC and E/I balance

The rsSC, as proposed by Fortel et al. [23, 49], is a hybrid connectivity combining structural and functional information. It aims to capture excitation-inhibition dynamics at a macroscopic level, especially in cases where regions show strong functional connectivity but lack direct structural links. This approach draws inspiration from the Ising model from statistical mechanics [50]. The Ising model was originally developed to model the (functional) interactions of magnetic dipoles arranged in a lattice. Precisely, it begins with a defined structural layout and infers binary functional states (spins) by minimizing the system's energy. Researchers have since applied the Ising model to the study of neural dynamics [51, 52]. The rsSC framework follows the inverse direction. It tries to infer the most suitable structural connectivity pattern that explains the observed functional states, a process known as structure-by-function embedding. The full algorithm details are presented in the Supplementary Material, section 1.**Figure** 1 illustrates the schematic of the pipeline, which is run for each of the studied parcelation atlases.

The resulting connectivity includes both positive and negative values representing macroscopically excitatory and inhibitory dynamics, respectively. Consequently, we calculate the E/I balance metric as the ratio between the number of positive and negative values in the rsSC. The computation is depicted in Eq. (1). Here, n_{positive} and n_{negative} are the number of positive and negative elements within the rsSC

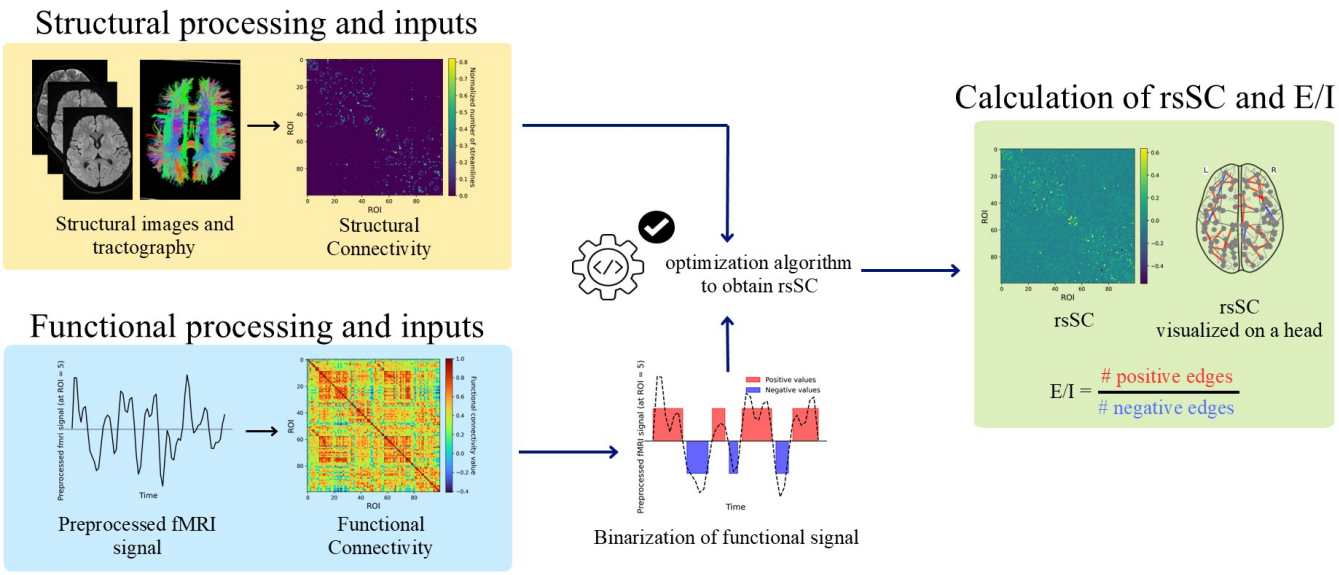

Figure 1. Pipeline to obtain the rsSC and the E/I metric We depict the pipeline for the calculation of the rsSC and the E/I metric. It takes as input the structural connectivity (in yellow block) and the binarized and preprocessed fMRI signals. The inputs are fed to a structure-by-function embedding, acting as the inverse process to the Ising model, and produce the rsSC. This multimodal matrix contains both positive and negative values. The E/I is calculated as the ratio of the number of positive and the number of negative values in the rsSC.

matrix, respectively.

$$\mathrm{E/I} = \frac{n_{\mathrm{positive}}}{n_{\mathrm{negative}}}. \tag{1}$$

The calculated metric serves as a bridge between microscale neural processes and large-scale network organization, helping to interpret how local activity influences the whole-brain connectivities. We investigate the excitation–inhibition (E/I) balance at global and at local network levels. After computing the E/I balance across all regions of interest (ROIs), we examine it within distinct resting-state networks (RSNs)—specifically, the default-mode network (DMN), the somatomotor network. For each RSN we calculate the E/I balance (EIB) under three conditions:

- **Intra-network:** connections among ROIs that belong to the same network. We obtain this metric from the upper triangle of the sub-matrix comprising only the ROIs of the network.
- **Inter-network:** connections between ROIs inside the network and ROIs outside it. This measure derives from the rectangular sub-matrix whose rows correspond to the network's ROIs and whose columns correspond to external ROIs.
- **Combined intra- and inter-network:** the union of the two previous sets of connections.

2.8 Statistical Analysis

To assess group differences in E/I balance between HC and pwMS, we used the Mann–Whitney U test, a non-parametric method appropriate for small sample sizes. Effect sizes were quantified with Cliff's δ, a rank-based measure estimating the probability that a value from one group exceeds one from the other. This metric is well-suited for small or unequal groups. To control for multiple comparisons, we applied FDR correction. Observations from different atlases were treated as independent; thus, for each atlas, we

corrected across the two RSNs and the three conditions (intra-, inter-, and combined intra–inter-network). After correction, $p < 0.05$ was considered significant.

3 RESULTS

3.1 Global E/I balance across the whole brain

After computing the rsSC matrices for each atlas (see Supplementary Material, section 2 for visual examples of structural, functional, and hybrid connectivity matrices), we calculated the global excitation/inhibition (E/I) balance (as in Eq. (1)) for both HCs and pwMS using all regions of interest (ROIs) in the hybrid rsSC matrix. **Figure** 2 shows the distribution of global E/I balance, calculated for all three brain parcellations (AAL, DK, and Schaefer). We found no statistically significant differences in E/I balance between groups for any of the atlases. Furthermore, the effect sizes were either negligible or small (see **Table** 2).

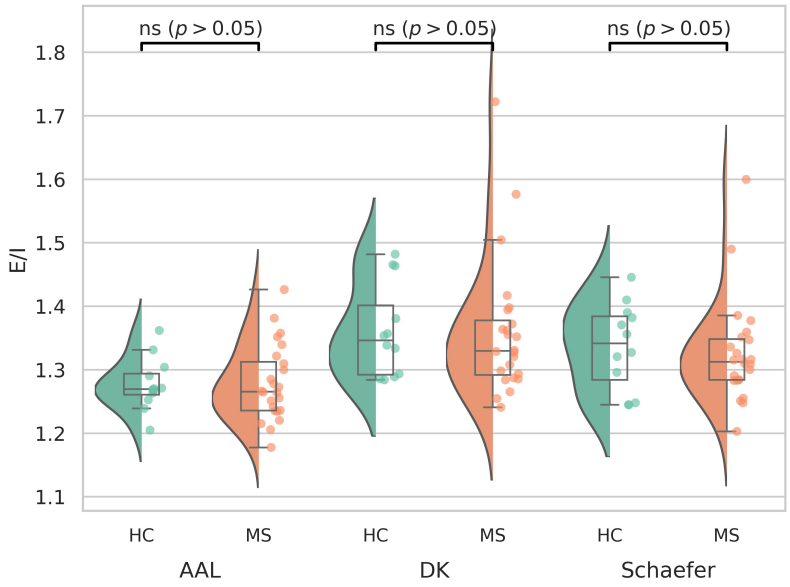

Figure 2. Violin plot of the E/I balance values computed across the whole brain, for HCs and pwMS. We show the violin plots of the E/I distributions computed across all ROIs for the three atlases (AAL, DK, and Scheafer) between the HC (in green) and pwMS (in orange). We do not observe significant differences between E/I balance values of HC and pwMS.

Table 2. Statistics for the differences in E/I values between HC and pwMS, calculated for ROIs over the whole head. We present the $p-$values from the Mann–Whitney U test and the corresponding Cliff's delta effect sizes for EIB values in the HC and pwMS groups, computed using the AAL, DK, and Schaefer atlases. We did not find any significant differences in EIB values between healthy controls and individuals with MS across any of the atlases. The associated effect sizes are either small or negligible.

	AAL	**DK**	**Schaefer**
$p-$value	0.46	0.63	0.89
Cliff's Delta effect size	0.15	0.099	-0.032

3.2 Local E/I balance calculated in the DMN and somatomotor network

Next, we analyzed the E/I balance within the somatomotor network and DMN. For each network, we first looked at intra-network E/I balance (see **Figures** 3(A) and 4(A) respectively). We found that the MS group had significantly lower E/I balance than the HC group in both networks after FDR correction, but only when using the Schaefer atlas (see **Figures** 3(B) and 4(B) respectively). The $p-$value and effect size for these analyses are reported in **Table** 3.

Table 3. Statistical analysis of EIB values in the somatomotor network and DMN across different brain atlases, comparing HCs and pwMS. EIB values were computed for the somatomotor and DMN network as defined by the AAL, Desikan–Killiany (DK), and Schaefer atlases. For each atlas, intra-network connections, inter-network connections, and combined intra- and inter-network connections were analyzed. Significant group differences were observed in intra-network EIB values for the Schaefer atlas for both the somatomotor and DMN. The associated effect sizes are large and medium.

	Somatomotor			**DMN**		
	AAL	**DK**	**Schaefer**	**AAL**	**DK**	**Schaefer**
Intra network						
$p-$value	0.68	1	0.016*	0.70	1	0.048*
Cliff's Delta effect size	0.57	0.25	0.54	0.38	-0.10	0.36
Inter network						
$p-$value	0.95	0.39	0.83	0.70	1	0.77
Cliff's Delta effect size	0.077	-0.17	-0.27	-0.15	0.35	-0.07
Intra and inter network						
$p-$value	0.95	0.39	0.85	0.70	1	0.83
Cliff's Delta effect size	0.077	-0.14	-0.20	-0.15	0.18	0.071

We then examined inter-network connections, defined as connections where only one ROI belongs to the network of interest (see **Figures** 3(C) and 4(C) respectively). In this case, the violin plots (see **Figures** 3(D) and 4(D) respectively) showed no significant differences, regardless of the atlas used. Finally, we analyzed the E/I values across all connections that included at least one node within the network **Figures** 3(E) and 4(E). This analysis did not show significant differences between networks or atlases (see **Figures** 3(F) and 4(F) respectively).

3.3 Correlation between E/I balance and clinical parameters in MS

We also examined whether intra-network E/I values in the DMN and somatomotor network were associated with cognitive and motor impairment. For the DMN, we assessed correlations with the FSMC–cognitive, COWAT, SDMT, and BVMT, computing Pearson coefficients after removing outliers. For the somatomotor network, we tested correlations with the FSMC–motor and EDSS. As shown in **Figure** 5, we found a significant negative correlation between FSMC–motor scores and somatomotor E/I balance. The correlation between FSMC–cognitive scores and DMN E/I values was also negative and approached significance ($p = 0.07$). No other correlations were significant. Full details are provided in section 4 of the Supplementary Material.

4 DISCUSSION

In this study, we applied a novel way to assess E/I balance in pwMS. The E/I balance is difficult to assess in vivo, and most studies on the E/I balance in MS rely on electroencephalography or

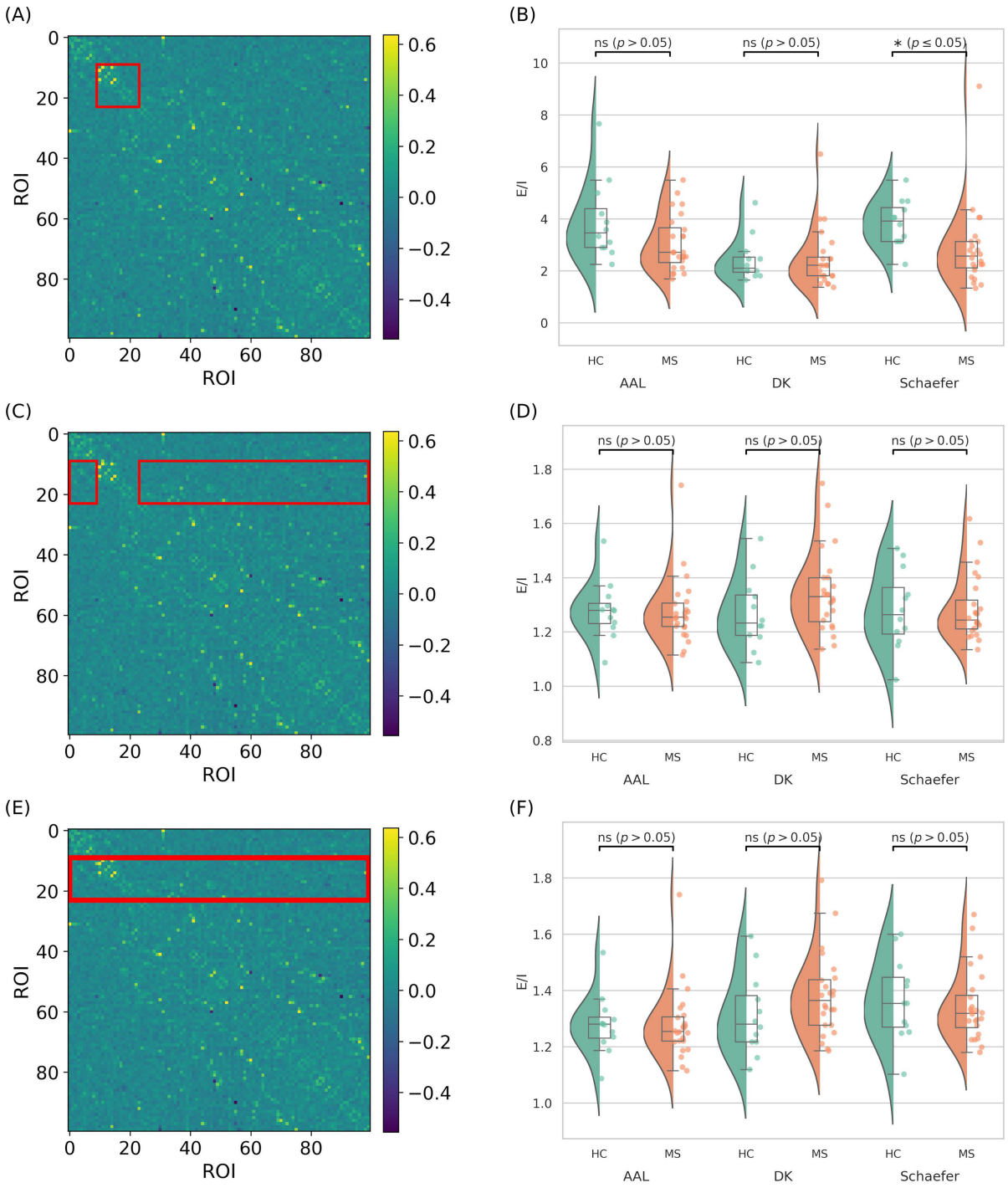

Figure 3. Illustration of the ROIs considered for the E/I calculation for the somatomotor network and statistical distribution of the computed metric between HC and pwMS group. We show the points considered on the rsSC, to calculate E/I in the somatomotor network for points that are (A) intra-network, (C) inter-network, and (E) both inter- and intra-network. On the side, we show the corresponding distribution of EIB values for: (B) ROIs within the somatomotor network, (D) inter-network connections involving the somatomotor network, and (F) both intra- and inter-network ROIs. Each analysis includes three brain atlases: Automated Anatomical Labeling (AAL), Desikan–Killiany (DK), and Schaefer. The Schaefer atlas shows significant differences ($p \leq 0.05$) after FDR correction for intra-network ROIs. We do not detect significant differences between healthy controls (HC) and people with multiple sclerosis (pwMS) when including inter-network connections.

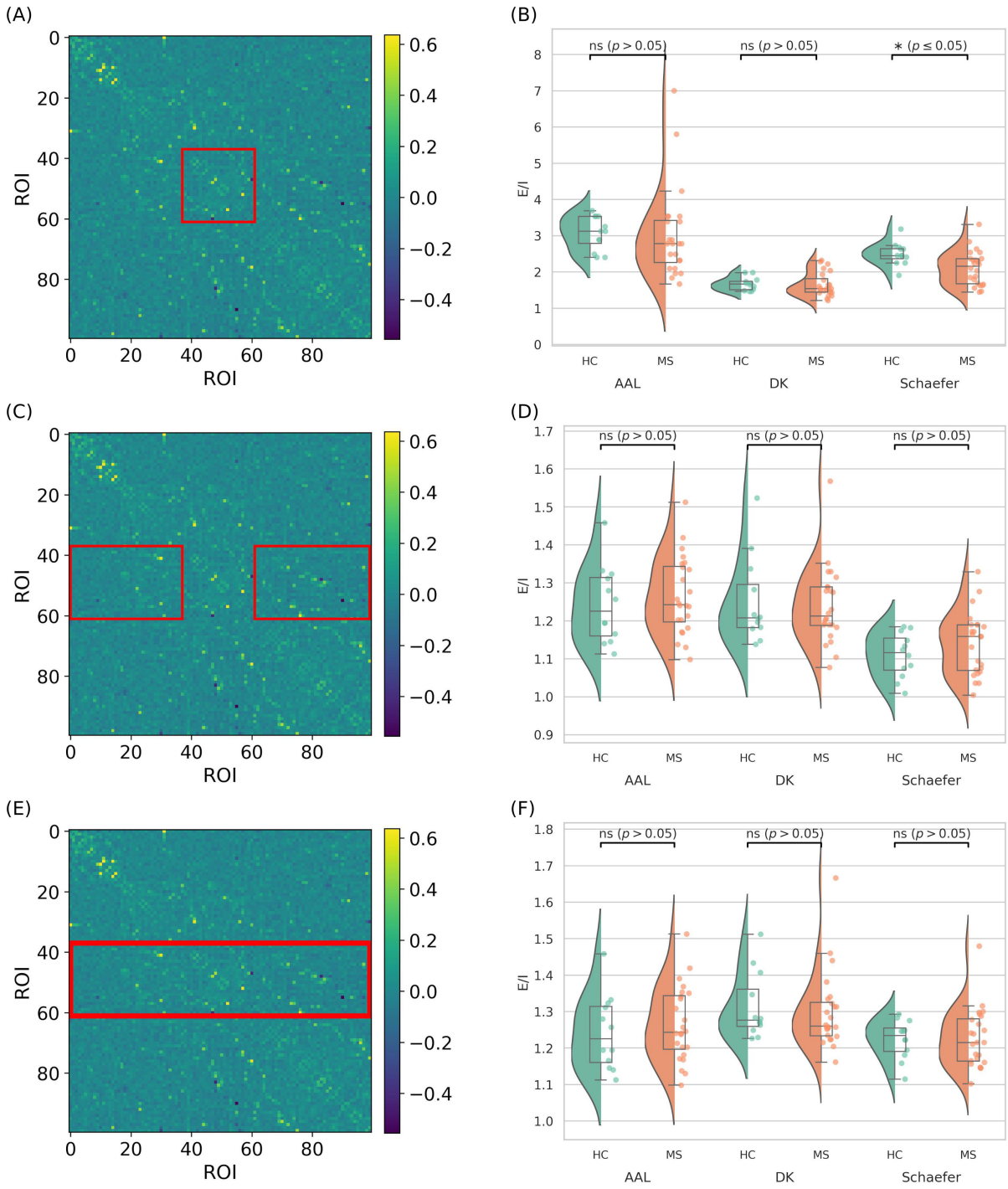

Figure 4. Illustration of the ROIs considered for the E/I calculation for the DMN and statistical distribution of the computed metric between HC and pwMS group. We show the points considered on the rsSC, to calculate E/I in the DMN network for points that are (A) intra-network, (C) inter-network, and (E) both inter- and intra-network. On the side, we show the corresponding distribution of EIB values for: (B) ROIs within the DMN, (D) inter-network connections involving the DMN, and (F) both intra- and inter-network ROIs. Each analysis includes three brain atlases: Automated Anatomical Labeling (AAL), Desikan–Killiany (DK), and Schaefer. The Schaefer atlas shows significant differences ($p \leq 0.05$) after FDR correction for intra-network ROIs. We do not detect significant differences between healthy controls (HC) and people with multiple sclerosis (pwMS) when including inter-network connections.

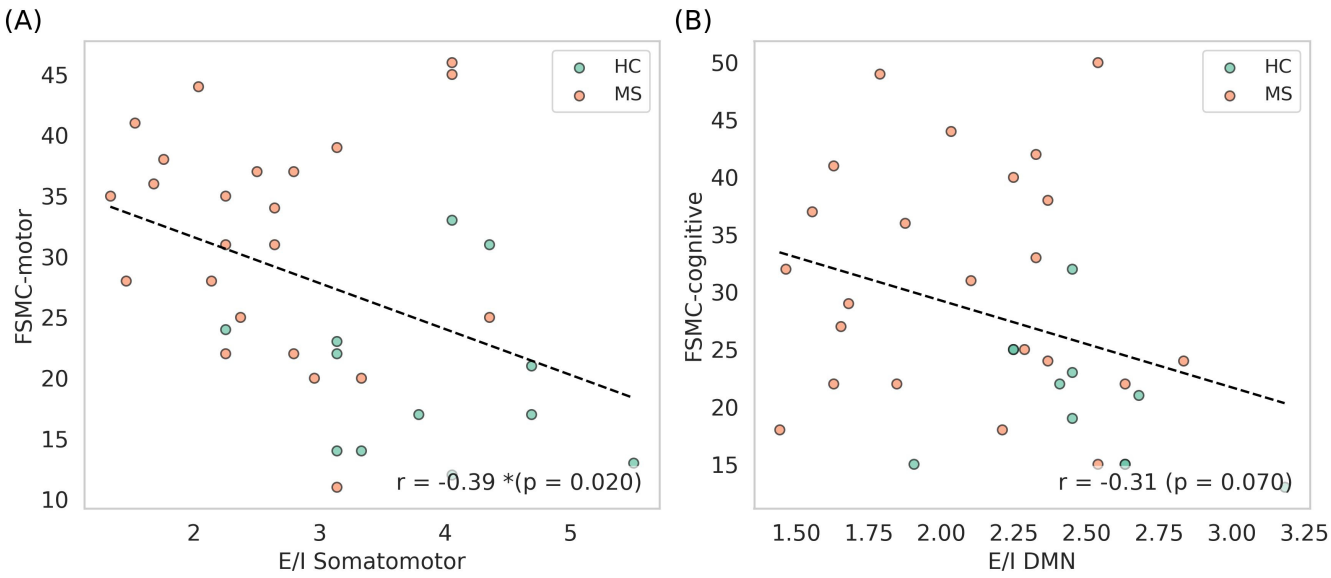

Figure 5. Scatter plots of the motor and cognitive components of the FSMC scores, plotted for each inferred E/I balance. In **(A)**, we show the motor component of the FSMC for each subject, with the E/I balance values from the intra-somatomotor network plotted on the horizontal axis. In **(B)**, a similar plot is shown using the cognitive component of the FSMC score and the E/I balance from the intra-DMN. In this visualization, outliers have been removed. The Pearson correlation coefficient for each plot is shown in the bottom right corner of the respective panel. The motor component of the FSMC shows a significant negative correlation with the E/I balance in the intra-somatomotor network.

magnetoencephalography. However, most neurofunctional studies in MS rely on fMRI. Here, we apply a recently proposed novel measure of E/I balance based on the so-called resting-state structural connectivity matrix. Similar to Fortel et al. [23], we defined the E/I balance as the ratio of positive (excitatory) to negative (inhibitory) connections in the rsSC matrix and studied it from a global and local perspective. In particular, we examined intra-network, inter-network, and combined connectivity within the somatomotor and DMN networks. Brain regions were defined using the functionally derived Schaefer atlas, which aligns with resting-state networks. For comparison, we also employed the Desikan–Killiany and AAL structural atlases to assess the influence of atlas choice on the results. Our findings highlight network-specific alterations in the E/I ratio in pwMS. These differences are network-specific and only appear within the DMN and somatomotor network. Precisely, alterations in E/I balance were not apparent inter-network or at a global level. In particular, intra-network DMN E/I exhibited a significant group difference ($p = 0.048$, FDR-corrected; medium effect size $= 0.36$), with the MS group showing lower E/I values than HC. This finding indicates a diminished excitatory drive or enhanced inhibitory tone during resting-state activity in pwMS. Similarly, our analysis reveals significant differences between HCs and pwMS for E/I intra-somatomotor network ($p = 0.016$, FDR corrected; large effect size $= 0.54$).

Previous studies examining E/I alterations specifically within the DMN in MS generally point to a loss of inhibitory tone. For example, a magnetic resonance spectroscopy study reported reduced GABA concentrations in DMN regions of patients with relapsing–remitting MS [53], although glutamatergic metabolites were not assessed. Additionally, Broeders et al. [54] observed greater functional instability in cognitively impaired MS patients compared with cognitively preserved individuals. They reported frequent reconfiguration of regions of interest into different resting-state networks, with the DMN showing particularly high levels of reconfiguration, an effect the authors interpreted as reflecting increased disinhibition within the DMN and consequently increased E/I balance. In contrast, our findings suggest

lower E/I values within the DMN in MS. Importantly, however, the E/I metric used here does not directly capture microscale neuronal or synaptic alterations [25]. Instead, it reflects large-scale connectivity changes that may arise downstream of cellular-level processes such as synaptic loss or shifts in the excitation–inhibition relationship. Thus, our measure may capture a macroscopic consequence of such processes rather than the processes themselves. Furthermore, we detected significant differences only for connections within the DMN, and not for those projecting outside the network. This could indicate that the effects are specific to the DMN, that they arise from interactions between the DMN and certain other networks, or that a larger sample size may be needed to identify effects involving the DMN and other brain regions.

Several studies of the somatomotor network in MS, primarily in animal models, have reported a pro-excitatory shift. For example, Potter et al. [17] found increased excitatory synapse density and loss of inhibitory interneurons in the primary somatomotor cortex, in experimental autoimmune encephalomyelitis. Other studies have also reported similar findings, see e.g., [55, 56, 57]. However, as for the DMN, our results capture a decrease intra-somatomotor network of E-I, describing a macroscopic effect. The employed method did not capture any significant alteration in E/I balance when including all connections involving the somatomotor network.

Furthermore, we observed all significant findings only when we used the Schaefer atlas. This is important because different atlases vary in how well they capture functional networks. We compared the Schaefer atlas with two structural atlases that researchers often use in fMRI studies and found that the functionally defined atlas detected differences more effectively when precise alignment with RSNs was critical. In contrast, anatomically based atlases such as DK and AAL showed lower sensitivity and often failed to detect network-specific functional changes.

Lastly, we examined the linear correlations between intra-network E/I values in the somatomotor network and DMN, computed using the Schaefer atlas, and clinical disability measures (Supplementary Material, **Figures** S7 and S8). The somatomotor intra-network E/I values showed a significant negative correlation with the FSMC motor component, indicating that lower E/I values are associated with greater motor fatigue.

One limitation of this study is the relatively small sample size, which reduces statistical power and limits generalizability. Future studies should include larger cohorts to validate and extend these findings. Additionally, investigating E/I balance during task-based paradigms, would be interesting, especially in relation to the DMN deactivation during working memory task.

5 CONCLUSIONS

This study highlights the potential of resting-state structural connectivity to infer E/I (im)balances in pwMS using MRI data alone. A significant reduction in E/I values was observed within the default mode and somatomotor networks of pwMS, suggesting a shift toward increased inhibitory influence within these systems. Furthermore, this reduction was significantly correlated with motor and cognitive fatigue. This pro-inhibitory alteration may reflect underlying neurophysiological adaptations or compensatory mechanisms associated with disease progression at a macroscopic level. The results suggest that functionally defined atlases might better highlight differences in this type of analysis.

CONFLICT OF INTEREST STATEMENT

The authors declare that the research was conducted in the absence of any commercial or financial relationships that could be construed as a potential conflict of interest.

FUNDING

GZ was supported by EUTOPIA PhD scholarship within the project "Leveraging neurocomputational models to extract the intracerebral conduction velocity as a novel non-invasive marker of information processing speed in MS".

ACKNOWLEDGMENTS

We gratefully acknowledge the fruitful discussions with Liang Zhan. We wish to thank Johan Baijot for the original versions of both the structural and functional pipeline and for the insightful conversations regarding them. The authors also thank all participants in this study for their commitment and participation.

DATA AVAILABILITY STATEMENT

Due to privacy regulations in accordance with the General Data Protection Regulation (EU) 2016/679, the MRI data from this study cannot be shared publicly. However, researchers interested in accessing the data for collaborative purposes are encouraged to reach out to the senior authors, Prof. Jeroen Van Schependom and Prof. Guy Nagels. The code to compute the hybrid rsSC connectomes ~~and E/I balance~~ can be found at: `https://github.com/iforte2/hybrid-connectome`

REFERENCES

[1]Browne P, Chandraratna D, Angood C, Tremlett H, Baker C, Taylor BV, et al. Atlas of multiple sclerosis 2013: a growing global problem with widespread inequity. *Neurology* **83** (2014) 1022–1024.

[2]Bove R, Chitnis T. Sexual disparities in the incidence and course of ms. *Clinical Immunology* **149** (2013) 201–210.

[3]Hemmer B, Kerschensteiner M, Korn T. Role of the innate and adaptive immune responses in the course of multiple sclerosis. *The Lancet Neurology* **14** (2015) 406–419.

[4]Haase S, Linker RA. Inflammation in multiple sclerosis. *Therapeutic advances in neurological disorders* **14** (2021) 17562864211007687.

[5]Chiaravalloti ND, DeLuca J. Cognitive impairment in multiple sclerosis. *The Lancet Neurology* **7** (2008) 1139–1151.

[6]Kinouchi O, Copelli M. Optimal dynamical range of excitable networks at criticality. *Nature physics* **2** (2006) 348–351.

[7]Bhatia A, Moza S, Bhalla US. Precise excitation-inhibition balance controls gain and timing in the hippocampus. *Elife* **8** (2019) e43415.

[8]Howes OD, Shatalina E. Integrating the neurodevelopmental and dopamine hypotheses of schizophrenia and the role of cortical excitation-inhibition balance. *Biological psychiatry* **92** (2022) 501–513.

[9]Anticevic A, Lisman J. How can global alteration of excitation/inhibition balance lead to the local dysfunctions that underlie schizophrenia? *Biological psychiatry* **81** (2017) 818–820.

[10]Scaduto P, Lauterborn JC, Cox CD, Fracassi A, Zeppillo T, Gutierrez BA, et al. Functional excitatory to inhibitory synaptic imbalance and loss of cognitive performance in people with alzheimer's disease neuropathologic change. *Acta neuropathologica* **145** (2023) 303–324.

[11]Burns AP, Fortel I, Zhan L, Lazarov O, Mackin RS, Demos AP, et al. Longitudinal excitation-inhibition balance altered by sex and apoe-ε4. *Communications Biology* **8** (2025) 488.

[12]Bruining H, Hardstone R, Juarez-Martinez EL, Sprengers J, Avramiea AE, Simpraga S, et al. Measurement of excitation-inhibition ratio in autism spectrum disorder using critical brain dynamics. *Scientific reports* **10** (2020) 9195.

[13]Nelson SB, Valakh V. Excitatory/inhibitory balance and circuit homeostasis in autism spectrum disorders. *Neuron* **87** (2015) 684–698.

[14]Huiskamp M, Kiljan S, Kulik S, Witte ME, Jonkman LE, GJM Bol J, et al. Inhibitory synaptic loss drives network changes in multiple sclerosis: an ex vivo to in silico translational study. *Multiple Sclerosis Journal* **28** (2022) 2010–2019.

[15]Oost W, Meilof JF, Baron W. Multiple sclerosis: what have we learned and can we still learn from electron microscopy. *Cellular and Molecular Life Sciences* **82** (2025) 1–22.

[16]Zoupi L, Booker SA, Eigel D, Werner C, Kind PC, Spires-Jones TL, et al. Selective vulnerability of inhibitory networks in multiple sclerosis. *Acta Neuropathologica* **141** (2021) 415–429.

[17]Potter LE, Paylor JW, Suh JS, Tenorio G, Caliaperumal J, Colbourne F, et al. Altered excitatory-inhibitory balance within somatosensory cortex is associated with enhanced plasticity and pain sensitivity in a mouse model of multiple sclerosis. *Journal of neuroinflammation* **13** (2016) 142.

[18]Akbarian F, Rossi C, Costers L, D'hooghe MB, D'haeseleer M, Nagels G, et al. The spectral slope as a marker of excitation/inhibition ratio and cognitive functioning in multiple sclerosis. *Human Brain Mapping* **44** (2023) 5784–5794.

[19]Fotiadis P, Parkes L, Davis KA, Satterthwaite TD, Shinohara RT, Bassett DS. Structure–function coupling in macroscale human brain networks. *Nature Reviews Neuroscience* **25** (2024) 688–704.

[20]Deco G, Jirsa VK, McIntosh AR. Emerging concepts for the dynamical organization of resting-state activity in the brain. *Nature reviews neuroscience* **12** (2011) 43–56.

[21]Batista-García-Ramó K, Fernández-Verdecia CI. What we know about the brain structure–function relationship. *Behavioral Sciences* **8** (2018) 39.

[22]Ajilore O, Zhan L, GadElkarim J, Zhang A, Feusner JD, Yang S, et al. Constructing the resting state structural connectome. *Frontiers in neuroinformatics* **7** (2013) 30.

[23]Fortel I, Butler M, Korthauer LE, Zhan L, Ajilore O, Driscoll I, et al. Brain dynamics through the lens of statistical mechanics by unifying structure and function. *International Conference on Medical Image Computing and Computer-Assisted Intervention* (Springer) (2019), 503–511.

[24]Fortel I, Butler M, Korthauer LE, Zhan L, Ajilore O, Sidiropoulos A, et al. Inferring excitation-inhibition dynamics using a maximum entropy model unifying brain structure and function. *Network Neuroscience* **6** (2022) 420–444.

[25]Fortel I, Zhan L, Ajilore O, Wu Y, Mackin S, Leow A. Disrupted excitation-inhibition balance in cognitively normal individuals at risk of alzheimer's disease. *Journal of Alzheimer's Disease* **95** (2023) 1449–1467.

[26]Manos T, Diaz-Pier S, Fortel I, Driscoll I, Zhan L, Leow A. Enhanced simulations of whole-brain dynamics using hybrid resting-state structural connectomes. *Frontiers in computational neuroscience* **17** (2023) 1295395.

[27]Schoonheim MM, Broeders TA, Geurts JJ. The network collapse in multiple sclerosis: An overview of novel concepts to address disease dynamics. *NeuroImage: Clinical* **35** (2022) 103108.

[28]Raichle ME. The brain's default mode network. *Annual review of neuroscience* **38** (2015) 433–447.

[29]Bonavita S, Gallo A, Sacco R, Corte MD, Bisecco A, Docimo R, et al. Distributed changes in default-mode resting-state connectivity in multiple sclerosis. *Multiple sclerosis journal* **17** (2011) 411–422.

[30]Rocca MA, Valsasina P, Absinta M, Riccitelli G, Rodegher M, Misci P, et al. Default-mode network dysfunction and cognitive impairment in progressive ms. *Neurology* **74** (2010) 1252–1259.

[31]Louapre C, Perlbarg V, García-Lorenzo D, Urbanski M, Benali H, Assouad R, et al. Brain networks disconnection in early multiple sclerosis cognitive deficits: an anatomofunctional study. *Human brain mapping* **35** (2014) 4706–4717.

[32]Vecchio F, Miraglia F, Porcaro C, Cottone C, Cancelli A, Rossini PM, et al. Electroencephalography-derived sensory and motor network topology in multiple sclerosis fatigue. *Neurorehabilitation and Neural Repair* **31** (2017) 56–64.

[33]Eto K, Wake H, Watanabe M, Ishibashi H, Noda M, Yanagawa Y, et al. Inter-regional contribution of enhanced activity of the primary somatosensory cortex to the anterior cingulate cortex accelerates chronic pain behavior. *Journal of Neuroscience* **31** (2011) 7631–7636.

[34]Kim SK, Nabekura J. Rapid synaptic remodeling in the adult somatosensory cortex following peripheral nerve injury and its association with neuropathic pain. *Journal of Neuroscience* **31** (2011) 5477–5482.

[35]Radetz A, Mladenova K, Ciolac D, Gonzalez-Escamilla G, Fleischer V, Ellwardt E, et al. Linking microstructural integrity and motor cortex excitability in multiple sclerosis. *Frontiers in Immunology* **12** (2021) 748357.

[36]Thompson AJ, Banwell BL, Barkhof F, Carroll WM, Coetzee T, Comi G, et al. Diagnosis of multiple sclerosis: 2017 revisions of the mcdonald criteria. *The Lancet Neurology* **17** (2018) 162–173.

[37]Tournier JD, Smith R, Raffelt D, Tabbara R, Dhollander T, Pietsch M, et al. Mrtrix3: A fast, flexible and open software framework for medical image processing and visualisation. *Neuroimage* **202** (2019) 116137.

[38]Smith SM, Jenkinson M, Woolrich MW, Beckmann CF, Behrens TE, Johansen-Berg H, et al. Advances in functional and structural mr image analysis and implementation as fsl. *Neuroimage* **23** (2004) S208–S219.

[39]Avants BB, Tustison NJ, Song G, Cook PA, Klein A, Gee JC. A reproducible evaluation of ants similarity metric performance in brain image registration. *Neuroimage* **54** (2011) 2033–2044.

[40]Pirzada S, Uddin MN, Figley TD, Kornelsen J, Puig J, Marrie RA, et al. Spatial normalization of multiple sclerosis brain mri data depends on analysis method and software package. *Magnetic resonance imaging* **68** (2020) 83–94.

[41]Ward HA, Riederer SJ, Grimm RC, Ehman RL, Felmlee JP, Jack Jr CR. Prospective multiaxial motion correction for fmri. *Magnetic Resonance in Medicine: An Official Journal of the International Society for Magnetic Resonance in Medicine* **43** (2000) 459–469.

[42]Power JD, Schlaggar BL, Petersen SE. Recent progress and outstanding issues in motion correction in resting state fmri. *Neuroimage* **105** (2015) 536–551.

[43]Schaefer A, Kong R, Gordon EM, Laumann TO, Zuo XN, Holmes AJ, et al. Local-global parcellation of the human cerebral cortex from intrinsic functional connectivity mri. *Cerebral cortex* **28** (2018) 3095–3114.

[44]Yeo BT, Krienen FM, Sepulcre J, Sabuncu MR, Lashkari D, Hollinshead M, et al. The organization of the human cerebral cortex estimated by intrinsic functional connectivity. *Journal of neurophysiology* (2011).

[45]Tzourio-Mazoyer N, Landeau B, Papathanassiou D, Crivello F, Etard O, Delcroix N, et al. Automated anatomical labeling of activations in spm using a macroscopic anatomical parcellation of the mni mri single-subject brain. *Neuroimage* **15** (2002) 273–289.

[46]Desikan RS, Ségonne F, Fischl B, Quinn BT, Dickerson BC, Blacker D, et al. An automated labeling system for subdividing the human cerebral cortex on mri scans into gyral based regions of interest. *Neuroimage* **31** (2006) 968–980.

[47]Lawrence RM, Bridgeford EW, Myers PE, Arvapalli GC, Ramachandran SC, Pisner DA, et al. Standardizing human brain parcellations. *Scientific data* **8** (2021) 78.

[48]Lee WH, Frangou S. Linking functional connectivity and dynamic properties of resting-state networks. *Scientific reports* **7** (2017) 16610.

[49]Fortel I, Korthauer LE, Morrissey Z, Zhan L, Ajilore O, Wolfson O, et al. Connectome signatures of hyperexcitation in cognitively intact middle-aged female apoe-ε4 carriers. *Cerebral Cortex* **30** (2020) 6350–6362.

[50]Cipra BA. An introduction to the ising model. *The American Mathematical Monthly* **94** (1987) 937–959.

[51]Tkacik G, Schneidman E, Berry II MJ, Bialek W. Ising models for networks of real neurons. *arXiv preprint q-bio/0611072* (2006).

[52]Das T, Abeyasinghe PM, Crone J, Sosnowski A, Laureys S, Owen A, et al. Highlighting the structure-function relationship of the brain with the ising model and graph theory. *BioMed research international* **2014** (2014) 237898.

[53]Cao G, Edden RA, Gao F, Li H, Gong T, Chen W, et al. Reduced gaba levels correlate with cognitive impairment in patients with relapsing-remitting multiple sclerosis. *European radiology* **28** (2018) 1140–1148.

[54]Broeders TA, Douw L, Eijlers AJ, Dekker I, Uitdehaag BM, Barkhof F, et al. A more unstable resting-state functional network in cognitively declining multiple sclerosis. *Brain Communications* **4** (2022) fcac095.

[55]Falco A, Pennucci R, Brambilla E, de Curtis I. Reduction in parvalbumin-positive interneurons and inhibitory input in the cortex of mice with experimental autoimmune encephalomyelitis. *Experimental brain research* **232** (2014) 2439–2449.

[56]Mandolesi G, Gentile A, Musella A, Centonze D. Il-1β dependent cerebellar synaptopathy in a mouse mode of multiple sclerosis. *The Cerebellum* **14** (2015) 19–22.

[57]Rossi S, Muzio L, De Chiara V, Grasselli G, Musella A, Musumeci G, et al. Impaired striatal gaba transmission in experimental autoimmune encephalomyelitis. *Brain, behavior, and immunity* **25** (2011) 947–956.

Supplementary Material

1 ALGORITHM FOR OBTAINING THE HYBRID RESTING-STATE STRUCTURAL CONNECTIVITY MATRICES

In this section, we describe the algorithm used to generate the hybrid (or signed) resting-state structural connectomes (rsSC), as presented in [1, 2, 3, 4, 5, 6]. This approach integrates structural connectivity with functional time-series data to construct a connectome that characterizes patterns of neural excitation and inhibition. An energy-based description of neural activity is constructed using the statistical-mechanics Ising model, avoiding reliance on standard BOLD correlation measures. In this framework, each pair of brain regions is represented by a coupling parameter (positive or negative) and corresponding spin states, while recorded functional time series capture the evolving brain states. The coupling parameters are estimated through constrained maximum pseudolikelihood, where the constraint acts as a penalty that scales inferred interactions according to structural connectivity. The sign of each estimated interaction can indicate inhibitory or excitatory influences on the underlying structural network.

The pipeline begins by binarizing the preprocessed and z-scored BOLD time series x_i at each ROI i according to $s_{i,t} = \text{sign}(x_{i,t})$. In this way, a brain region i is considered active if $s_i = +1$ and inactive if $s_i = -1$. This step links the functional time series to the spin states of the Ising model. We write the vector of states at time t as $\mathbf{s} = [s_1, s_2, \ldots, s_k]$, where k is the number of ROIs. The time series is first standardized using $z-$score normalization to achieve zero mean and unit variance. Because the interaction term (denoted as $J_{i,j}$ between two regions should correspond to their structural connectivity derived from diffusion MRI tractography, we impose a constraint on the Hamiltonian:

$$H(\mathbf{s}) = \sum_{i<j} J_{i,j} s_i s_j \tag{S1}$$

such that $|J_{i,j}| \propto W_{i,j}$, where $(W_{i,j})$ denotes the structural connectivity (weights) between each pair of ROIs. For resting-state data, external fields are omitted. This formulation ensures that during pseudolikelihood estimation, the inferred interaction matrix J is guided by structural connectivity, assuming that anatomy shapes the spin dynamics. The optimal J is then obtained by maximizing the pseudolikelihood function. Then, the optimal interaction matrix $\mathbf{J}$ is obtained by maximizing the probability function $Pr(\mathbf{s})$ of observing the (functional) states $\mathbf{s}$ at time t. The pseudolikelihood function is defined as:

$$\mathcal{L}_{\text{pseudo}}(\mathbf{J}, \beta) = \prod_{t=1}^{t_{\max}} \prod_{i=1}^{k} \Pr\left(s_i(t) \mid \mathbf{J}, \beta, \mathbf{s}_{-i}(t)\right). \tag{S2}$$

Here, $Pr(\mathbf{s})$ is approximated by the product of the conditional probabilities $\tilde{p} = \Pr\left(s_i(t) \mid \mathbf{J}, \beta, \mathbf{s}_{-i}(t)\right)$ of observing the state $s_i(t)$ given all the other states $\mathbf{s}_{-i}(t)$, the interaction matrix $\mathbf{J}$ and the variable β representing the temperature of the system (from the Ising model). We also note that t_{max} depends on the duration of the fMRI series. The log-pseudolikelihood with this penalty term is:

$$\ell(\mathbf{J}, \beta) = \frac{1}{t_{\max}} \ln \mathcal{L}_{\text{pseudo}}(\mathbf{J}, \beta) - \frac{\lambda}{2} \sum_{i<j} \left(J_{i,j} - \text{sgn}(J_{i,j}) W_{i,j}\right)^2.$$

The pseudolikelihood component expands as follows:

$$\frac{1}{t_{\max}} \ln \mathcal{L}_{\text{pseudo}}\left(\mathbf{J},\beta\right) = \frac{1}{t_{\max}} \sum_{t=1}^{t_{\max}} \sum_{i=1}^{N} \ln\left(\frac{\exp(\beta \sum_{k=1}^{N} J_{i,k} s_i(t) s_k(t))}{\exp(\beta \sum_{k=1}^{N} J_{i,k} s_k(t)) + \exp(-\beta \sum_{k=1}^{N} J_{i,k} s_k(t))}\right). \tag{S3}$$

This method relies on the Boltzmann distribution under pseudolikelihood assumptions. The numerator captures the system's energy, while the denominator sums over all possible energy states. With si(t) taking on only two binary values, the denominator consists of just two terms—one for each possible sign. The likelihood expression can therefore be simplified by setting: $C_i(t) = \beta \sum_{m=1}^{k} J_{i,m} s_m(t)$, resulting in:

$$\begin{aligned}\ell(\mathbf{J},\beta) = \frac{1}{t_{\max}} \sum_{t=1}^{t_{\max}} \sum_{i=1}^{N} C_i(t) s_i(t) - \ln(\exp(C_i(t)) + \exp(-C_i(t))) - \\ - \frac{\lambda}{2} \sum_{i<j} (J_{i,j} - \text{sgn}(J_{i,j} W_{i,j}))^2.\end{aligned} \tag{S4}$$

After defining $C_i(t) = \beta \sum_{m=1}^{k} J_{i,m} s_m(t)$ and we can formulate the probability distribution of the states using the Boltzmann distribution under pseudolikelihood condition. In this way, we can rewrite Eq. (S3) as:

$$\begin{aligned}\ell(\mathbf{J},\beta) = \frac{1}{t_{\max}} \sum_{t=1}^{t_{\max}} \sum_{i=1}^{N} \left(C_i(t) s_i(t) - \ln\left(\exp(C_i(t)) + \exp(-C_i(t))\right)\right) \\ - \frac{\lambda}{2} \sum_{i<j} \left(J_{i,j} - \text{sgn}(J_{i,j}) W_{i,j}\right)^2.\end{aligned} \tag{S5}$$

Finally, to optimize the matrix $\mathbf{J}$, we apply the gradient ascent method:

$$\frac{\partial \ell}{\partial J_{i,j}} = \frac{1}{t_{\max}} \sum_{t=1}^{t_{\max}} \beta \left\{s_i(t) s_j(t) - s_j(t) \tanh(C_i(t))\right\} - \lambda \left(J_{i,j} - \text{sgn}(J_{i,j}) W_{i,j}\right) \tag{S6}$$

$$\propto \frac{1}{t_{\max}} \sum_{t=1}^{t_{\max}} \left\{s_i(t) s_j(t) - s_j(t) \tanh(C_i(t))\right\} - A \left(J_{i,j} - \text{sgn}(J_{i,j}) W_{i,j}\right). \tag{S7}$$

In this last equation $A = \lambda/\beta$. The update rule for the interaction matrix is:

$$J_{i,j}^{n+1} = J_{i,j}^{n} + \gamma \left.\frac{\partial \ell}{\partial J_{i,j}}\right|_{n}. \tag{S8}$$

Here, n is the iteration number, and γ is the learning rate. The estimated matrix $\mathbf{J}$ represents the resting-state structural connectivity (rsSC), or hybrid connectivity. Next, the pipeline optimizes the parameters A and β. Two metrics guide this process. The first metric, $r_{\text{structural}}$, is the Pearson correlation between the rsSC and the empirical structural connectivity ($\mathbf{W}$). The second metric, $r_{\text{functional}}$, is the correlation between the empirical functional connectivity and the simulated one. The simulated functional connectivity is obtained by using the rsSC as input to Markov Chain Monte Carlo-based Ising model simulations. The values of $r_{\text{structural}}$ and $r_{\text{functional}}$ are computed for different combinations of A and β values. A grid search then

identifies the optimal parameters giving max $r_{\text{structural}} + r_{\text{functional}}$. This procedure gives equal weight to the reconstruction of structural and functional.

2 EXAMPLES OF FUNCTIONAL, STRUCTURAL AND HYBRID RESTING-STATE STRUCTURAL CONNECTIVITY MATRICES

In this section, we provide examples of the three types of connectivity matrices (functional, structural and hybrid) that are used in this project. In **Figure** S1, we show the three different connectivity matrices for the three different atlases considered (AAL, DK and Schaefer) for a Healthy Control subject.

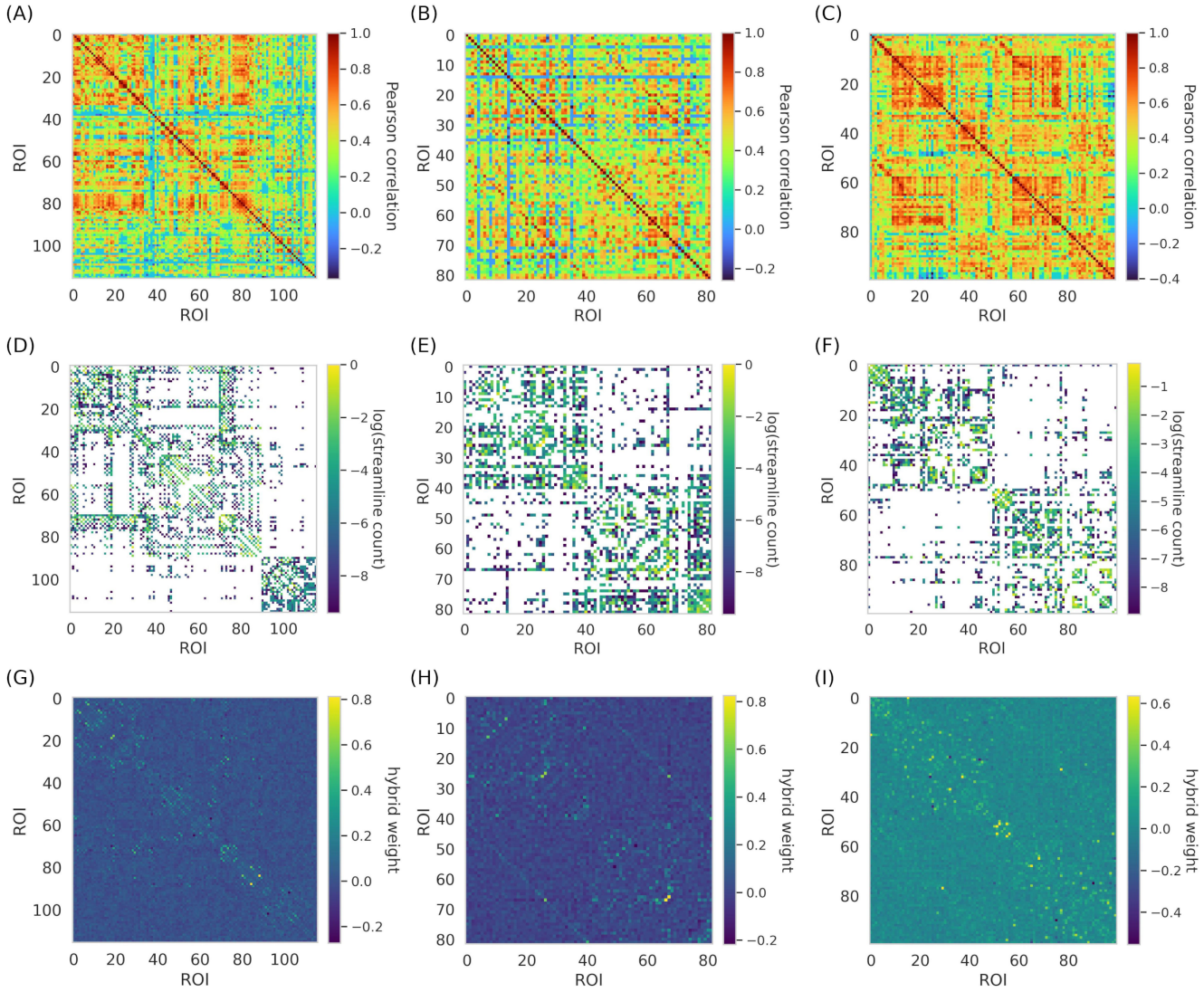

Figure S1. Functional, structural and rsSC of one HC subject, for every considered atlas. (A), (B), (C) show the functional connectivity matrices of one healthy control (HC) subject using the AAL, DK, and Schaefer atlases. (D), (E), (F) show the corresponding structural connectivity matrices. We normalize all matrices and plot their logarithmic values for visualization. (G), (H), (I) show the resulting hybrid rsSC matrices for the same atlases.

3 RESTING STATE FUNCTIONAL NETWORKS IN THE AAL ATLAS

The structural atlases do not have a direct link to functional networks. Hence, we overlap the AAL with the Yeo7 atlas and we study their overlap [7]. Precisely, we calculate the percentage of voxels in the AAL ROI i_{AAL} belonging to the Yeo area i_{Yeo} (**Figure** S2). In **Figure** S4, we study how the Somatomotor networks look on the AAL atlas for the minimum percentage of overlap of 10%, 20%, and 30%. The somatomotor network is composed of a unique 'band' that can be well represented with a percentage of overlap of 30% (**Figure** S4). We note that higher percentages can be investigated as well, taking into account that they would cause the loss of more areas **(Figure** S3. For the DMN, we choose an overlap of 30% as it seems to be well represented **(Figure** S5.

The structural atlases do not directly correspond to functional networks. Therefore, we overlap the AAL atlas with the Yeo7 atlas and analyze their overlap [**?**]. Specifically, we calculate the percentage of voxels in each AAL ROI i_{AAL} that belong to each Yeo network i_{Yeo} **(Figure** S2). In **Figure** S4, we examine how the somatomotor networks are represented on the AAL atlas, using minimum overlap percentages of 10%, 20%, and 30%. The somatomotor network forms a distinct "band" that is most clearly represented with a 30% overlap (**Figure** S4). Higher overlap percentages could also be explored, though they would result in the loss of more areas (**Figure** S3). For the Default Mode Network (DMN), we use a 30% overlap, as it provides a clear representation (**Figure** S5).

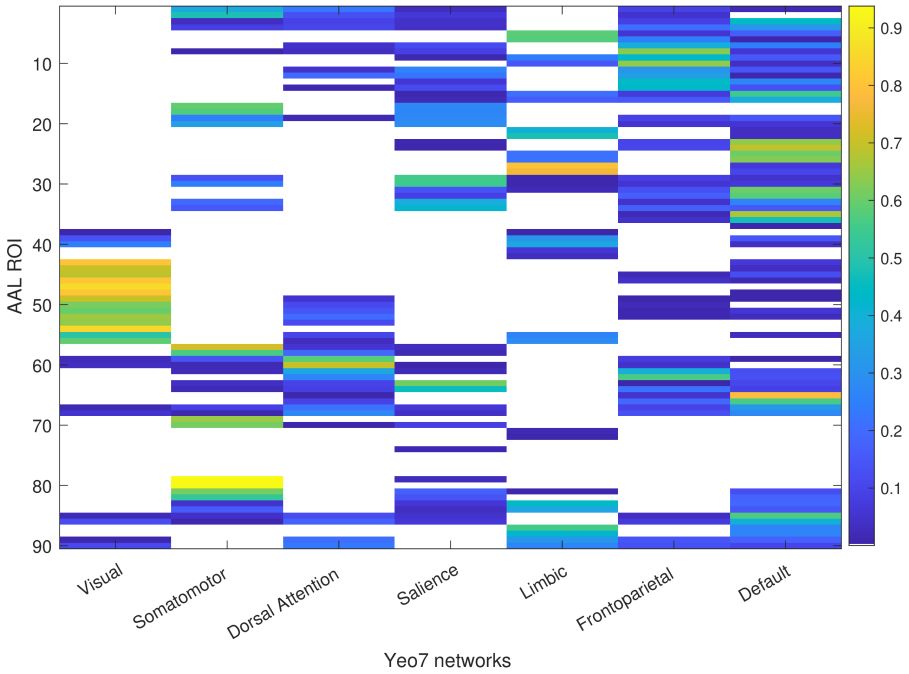

Figure S2. Overlap between AAL ROIs and Yeo7 Networks. This analysis reports the percentage of voxels in each AAL ROI that overlap with the seven Yeo functional networks.

Then, we investigate different thresholds of overlap. This means that we study what happens when imposing a minimum percentage of overlap $p_{\text{threshold}}$. In **Figure** S3, we look at how $p_{threshold}$ influences the number of AAL ROIs for the three Yeo networks considered in the previous analysis.

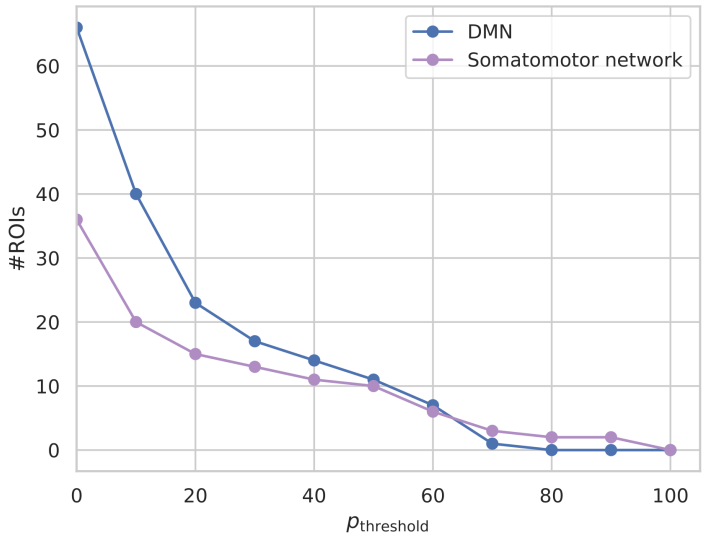

Figure S3. Analysis of number of AAL ROIs with minimal percentage of overlap with relevant RSNs. This analysis examines the overlap between AAL ROIs and the DMN and somatomotor network as defined by the Yeo7 atlas. We calculate the percentage of voxels overlapping with the DMN for each AAL ROI. We then count how many ROIs exceed a defined threshold of overlap. This approach helps exclude regions with only marginal involvement in the network.

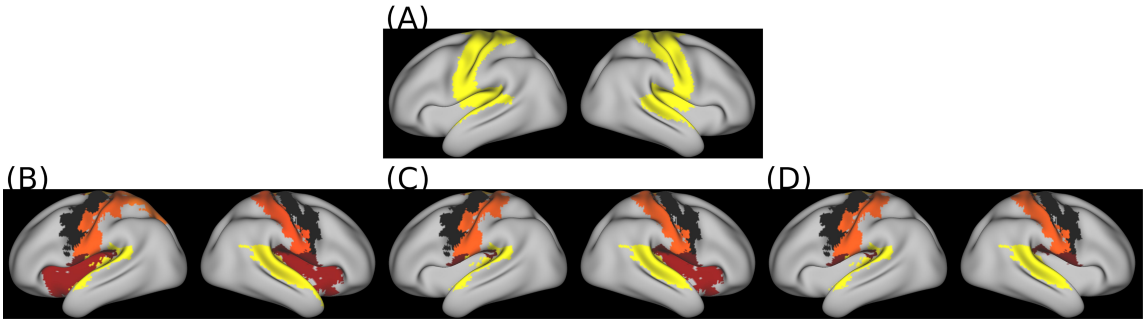

Figure S4. Somatomotor network mapped onto the AAL atlas, using varying minimal overlap thresholds. (A) The somatomotor network from the Yeo7 atlas is shown on an inflated brain surface. (B), (C), (D) AAL regions that show at least 10%, 20%, and 30% voxel overlap, respectively, with the somatomotor network from the Yeo7 atlas.

4 LINKING EXCITATION INHIBITION BALANCE TO MULTIPLE SCLEROSIS CLINICAL PARAMETERS

We investigated the association between the inferred intra-network E/I values in the DMN and somatomotor network and clinical measures of cognitive and motor impairment. We quantified these associations using the Pearson correlation coefficient after removing outliers. To remove outliers, we applied a data-driven approach based on the interquartile range. Specifically, we excluded data points whose residuals (to the regression line) fell outside the intervale between $Q1 - 1.5 * IQR$ and $Q3 + 1.5 * IQR$ with $Q1$ and $Q3$ being the first and third quartiles, respectively.

For the DMN, we evaluated correlations with the cognitive subscale of the Fatigue Scale for Motor and Cognitive Functions (FSMC–cognitive), the Controlled Oral Word Association Test (COWAT), the

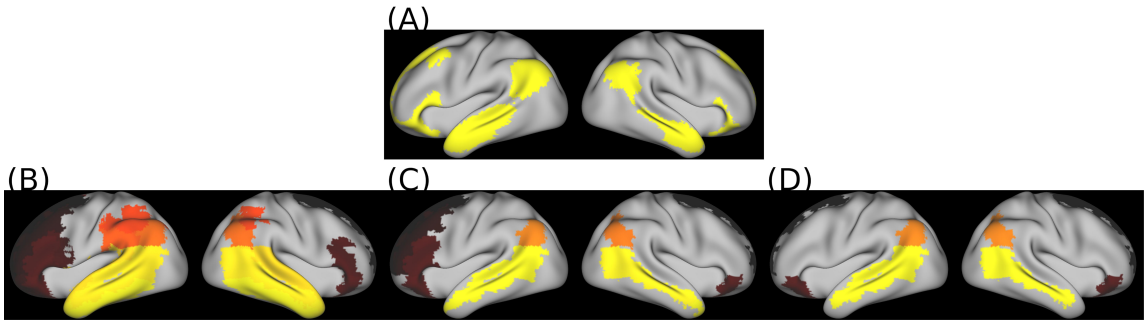

Figure S5. Default mode network mapped onto the AAL atlas, using varying minimal overlap thresholds. (A) The DMN from the Yeo7 atlas is shown on an inflated brain surface. (B), (C), (D) AAL regions that show at least 10%, 20%, and 30% voxel overlap, respectively, with the DMN from the Yeo7 atlas.

Symbol Digit Modalities Test (SDMT), and the Brief Visuospatial Memory Test–Revised (BVMT). For visualization, we indicate whether each E/I value belongs to the HC group (green) or the patient group (orange), although the correlation analysis includes all participants. The points indicated in grey (in the correlation with the FsMC-cognitive and BVMT scores) are the outliers identified by our data-driven algorithm. In both cases, the outlier belonged to the MS group. We did not observe any statistically significant correlations.

For the somatomotor network, we examined correlations with the FSMC-motor and the Expanded Disability Status Scale (EDSS). **Figure** S7 presents these results. An outlier belonging to the MS group was also identified for the correlation with the FSMC-motor and EDSS scores. This analysis revealed a statistically significant negative correlation between the inferred E/I values and the FSMC-motor scores.

REFERENCES

[1]Ajilore O, Zhan L, GadElkarim J, Zhang A, Feusner JD, Yang S, et al. Constructing the resting state structural connectome. *Frontiers in neuroinformatics* **7** (2013) 30.

[2]Fortel I, Butler M, Korthauer LE, Zhan L, Ajilore O, Driscoll I, et al. Brain dynamics through the lens of statistical mechanics by unifying structure and function. *International Conference on Medical Image Computing and Computer-Assisted Intervention* (Springer) (2019), 503–511.

[3]Fortel I, Korthauer LE, Morrissey Z, Zhan L, Ajilore O, Wolfson O, et al. Connectome signatures of hyperexcitation in cognitively intact middle-aged female apoe-ε4 carriers. *Cerebral Cortex* **30** (2020) 6350–6362.

[4]Fortel I, Butler M, Korthauer LE, Zhan L, Ajilore O, Sidiropoulos A, et al. Inferring excitation-inhibition dynamics using a maximum entropy model unifying brain structure and function. *Network Neuroscience* **6** (2022) 420–444.

[5]Fortel I, Zhan L, Ajilore O, Wu Y, Mackin S, Leow A. Disrupted excitation-inhibition balance in cognitively normal individuals at risk of alzheimer's disease. *Journal of Alzheimer's Disease* **95** (2023) 1449–1467.

[6]Burns AP, Fortel I, Zhan L, Lazarov O, Mackin RS, Demos AP, et al. Longitudinal excitation-inhibition balance altered by sex and apoe-ε4. *Communications Biology* **8** (2025) 488.

[7]Van Geest Q, Douw L, Van't Klooster S, Leurs C, Genova H, Wylie G, et al. Information processing speed in multiple sclerosis: Relevance of default mode network dynamics. *NeuroImage: Clinical* **19** (2018) 507–515.

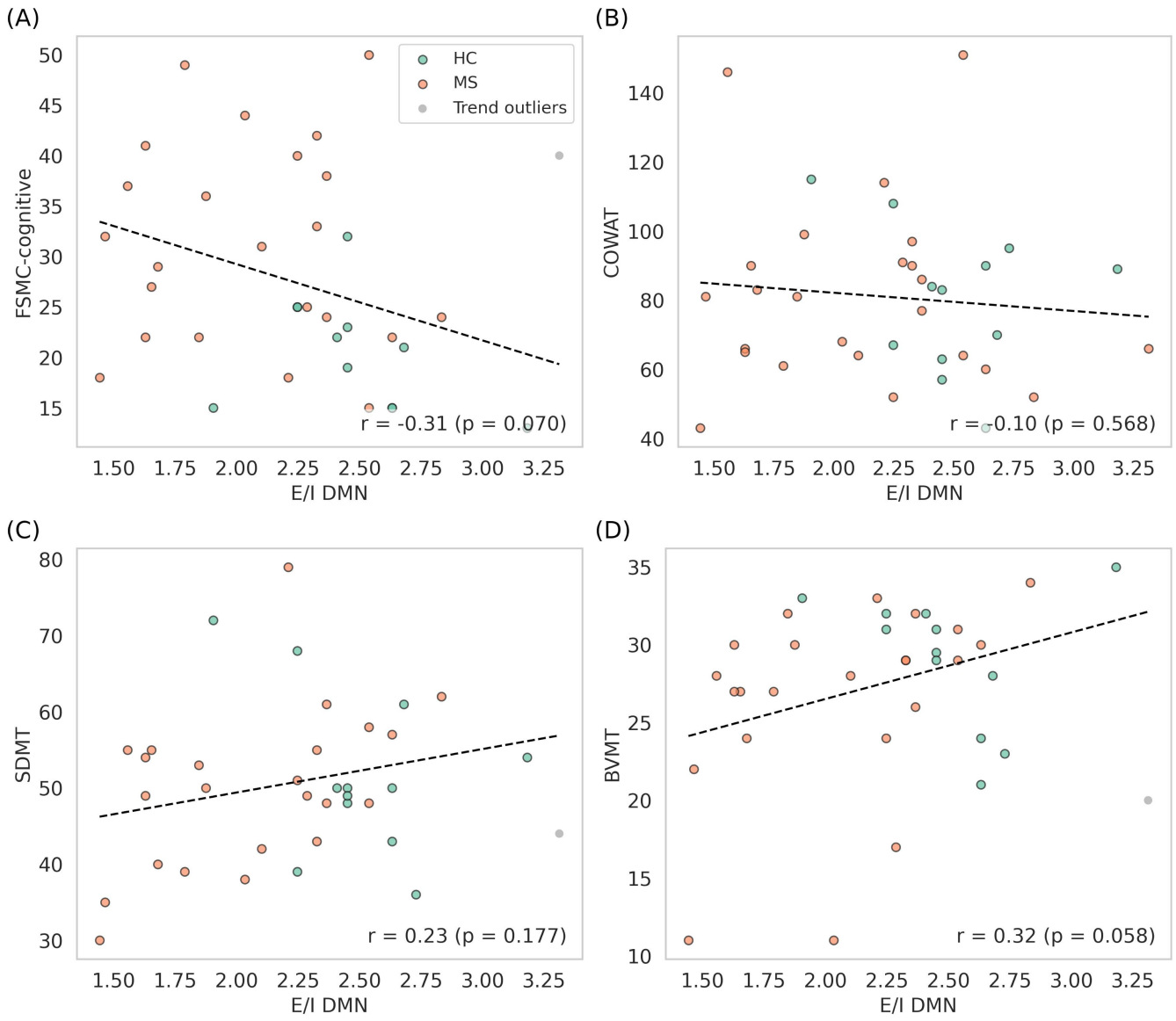

Figure S6. Correlation analysis between E/I balance in the DMN and cognitive clinical measures. Pearson correlation coefficient between intra-network E/I values in the DMN and (A) FSMC (cognitive), (B) COWAT, (C) SDMT, and (D) BVMT scores. Grey points indicate outliers removed before the analysis. We found no statistically significant correlations.

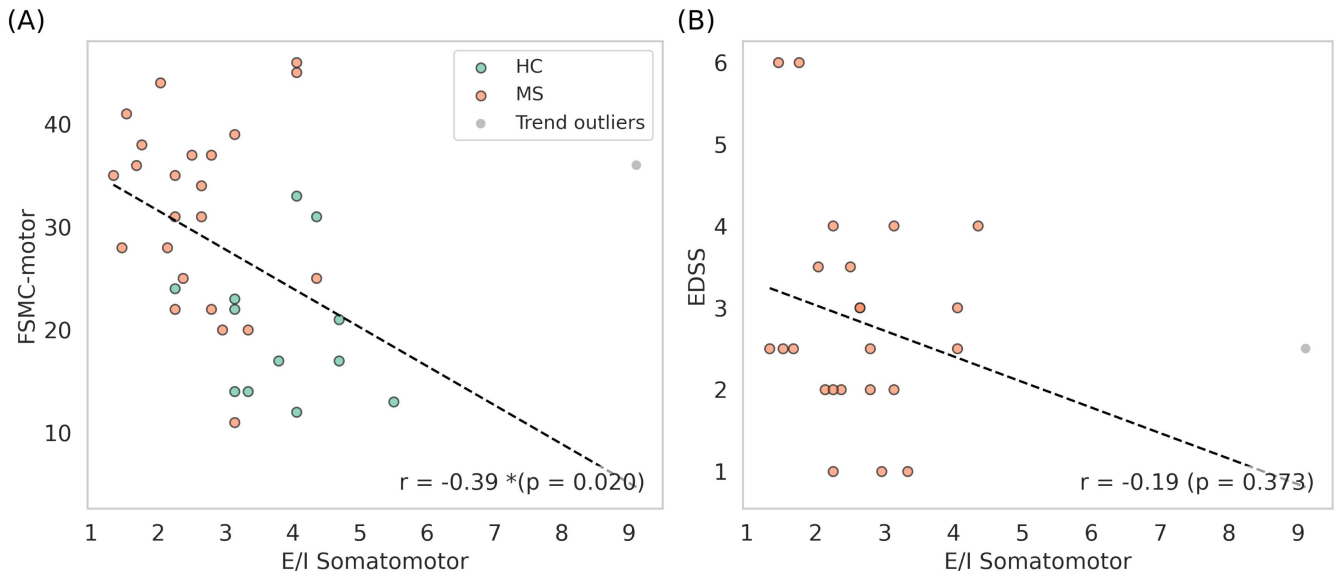

Figure S7. Correlation analysis between E/I balance in the somatomotor network and motor impairment. Pearson correlation coefficient between intra-network E/I values in the somatomotor network and (A) FSMC (motor) and (B) EDSS scores. Grey points indicate outliers removed before the analysis. We found a statistically significant negative correlation with the FSMC (motor) score.